JGR Space Physics

RESEARCH ARTICLE
10.1029/2022JA030629

Key Points:

- Continuous enhancements of electron temperature in the subauroral ionosphere over 8 days are observed and reported for the first time
- Hemispheric symmetry of electron temperature enhancement in the post-midnight sector and hemispheric asymmetry near dawn are identified
- Large daily variations of maximum electron temperature at subauroral latitudes are observed

Correspondence to:
C.-S. Huang,
chaosong.huang.1@spaceforce.mil

Citation:
Huang, C.-S., Zhang, Y., Wang, W., Wu, Q., & Lin, D. (2022). Continuous enhancements of electron temperature in the subauroral ionosphere over eight days during the 2015 St. Patrick's day storm. *Journal of Geophysical Research: Space Physics*, *127*, e2022JA030629. https://doi.org/10.1029/2022JA030629

Received 6 MAY 2022
Accepted 5 AUG 2022

Continuous Enhancements of Electron Temperature in the Subauroral Ionosphere Over Eight Days During the 2015 St. Patrick's Day Storm

Chao-Song Huang[1], Yongliang Zhang[2], Wenbin Wang[3], Qian Wu[3], and Dong Lin[3]

[1]Space Vehicles Directorate, Air Force Research Laboratory, Kirtland AFB, NM, USA, [2]Applied Physical Laboratory, Johns Hopkins University, Laurel, MD, USA, [3]National Center for Atmospheric Research, Boulder, CO, USA

Abstract We have used measurements of the Defense Meteorological Satellite Program (DMSP) satellites to study variations of electron temperature in the subauroral ionosphere during the magnetic storm on 17–25 March 2015. This magnetic storm had a long recovery phase of 7 days, and the ionospheric behavior over the entire storm time was seldom investigated. In this study, we find that the electron temperature at subauroral latitudes was continuously enhanced for 8 days, from the storm onset to the end of the recovery phase. The maximum electron temperature during the storm times was 1000–4000 K higher than the maximum electron temperature during quiet times. This long-lasting enhancement of subauroral electron temperature was attributed to energy transfer among the solar wind, magnetosphere, ring current, plasmasphere, and ionosphere driven by high-speed solar wind streams and fluctuating interplanetary magnetic field during the entire 8-day period of the storm. The electron temperature enhancements were quite symmetric in the post-midnight sector but became strongly asymmetric near dawn between the southern and northern hemispheres. The asymmetric enhancements of electron temperature near dawn may be related to the magnetic declination and the daytime midlatitude trough in the southern hemisphere. Large daily variations of maximum electron temperature in the post-midnight sector were observed and may be related to the offset between geomagnetic and geographic latitudes. These DMSP observations provide new insight on ionospheric response to intense magnetic storms.

1. Introduction

The subauroral ionosphere has unique features that are different from other regions of the ionosphere. One feature is the occurrence of strong westward plasma drifts in the dusk-midnight sector during magnetic storms and substorms. The storm-time (or substorm-time) westward plasma drifts, termed subauroral polarization streams (SAPS), can reach 1000 m s^{-1} or higher, cover several degrees in latitude, and last for many hours (Anderson, 2004; Foster, 1993; Foster & Burke, 2002; Foster & Vo, 2002). During geomagnetic active periods, enhanced region-2 field-aligned currents (R2 FACs) flow into the ionosphere in the afternoon-evening sector and close with the out flowing region-1 (R1) FACs, leading to the generation of poleward Pederson currents and electric fields between the two current sheets (Anderson et al., 1993). The westward E × B drifts associated with the poleward electric fields cause increased frictional heating and recombination, leading to further decrease of the ionospheric Pedersen conductivity and increase of the poleward electric fields (Foster & Burke, 2002; Mishin & Burke, 2005). Such a positive feedback process results in the generation of strong SAPS flows. Recent studies show that duskside SAPS penetrate to equatorial latitudes, causing westward plasms drifts (Huang, 2020; Huang et al., 2021). Enhanced subauroral electric fields in the dawnside are also identified from multi-satellite measurements (Horvath & Lovell, 2021), and the dawnside SAPS penetrates to middle and low latitudes, causing eastward plasma drifts (Huang et al., 2021).

Another unique feature of the subauroral ionosphere is significant enhancement of electron temperature during magnetic storms. During storm times, energetic particles are injected from the magnetotail into the inner magnetosphere and the ring current. The ring current particles are a major heat source for the thermal plasma in this region (Prölss, 2006). The plasmasphere, especially the plasmapause, sometimes overlaps with the ring current, and energy is transferred from the hot ring current ions to the cold plasmaspheric particles. The primary energy transfer channel is through Coulomb collisions (Kozyra et al., 1987), and wave–particle interactions may also play an important role (Cornwall et al., 1971; Thorne & Horne, 1992). Energy in the ring current-plasmasphere is transferred to the ionosphere through soft particle precipitation along magnetic field lines, causing ionospheric

electron temperature enhancements at subauroral latitudes. Brace et al. (1974, 1988), using satellite measurements in the *F* region, found a peak in electron temperature at night on the *L* shells that were magnetically connected to the equatorial plasmapause and attributed the ionospheric electron temperature enhancement to heating by magnetospheric sources. Kozyra et al. (1986) analyzed data from the DE-2 satellite over 488 passes through the plasmapause region during 1981 and did a statistical study of the *F*-region subauroral electron temperature enhancement. They identified a dependence of the peak electron temperature on the Dst and Kp indices. Prölss (2006) showed that the location (latitude) of the electron temperature enhancement is primarily controlled by the level of geomagnetic activity and also depends on magnetic local time. The studies of Brace et al. (1974, 1988) and Kozyra et al. (1986) showed that there is a positive height gradient in the nighttime subauroral ionospheric electron temperature, implying a high altitude heat source from the ring current. On the other hand, the positive feedback mechanism in the generation of SAPS could boost the plasma density depletion in the ionospheric ionization trough and lead to electron temperature increase because of the anti-correlation between plasma density and electron temperature, contributing to the subauroral electron temperature enhancements to some extent.

The electron temperature in the topside ionosphere is determined primarily by photoelectron heating on the dayside or heating from particle precipitation on the nightside, cooling by collisions with ions and neutrals, and heat conduction along magnetic field lines (Schunk & Nagy, 1978). Heat conduction from the topside electrons to the electrons at lower altitudes can be important in the night-time ionization trough because plasma density is low there, especially during magnetic storms. The dissociative recombination coefficient of ionospheric ions and electrons depends on electron temperature (Schunk & Nagy, 1980). A high electron temperature reduces the recombination rate and acts to increase the electron density and thereby ionospheric conductivity. On the other hand, electrons lose energy in Coulomb collisions with ions, and higher plasma density leads to higher electron energy loss (lower electron temperature). The electron temperature is related to the ionospheric plasma density and conductivity through these processes. The poleward electric fields in the SAPS region are determined by the R1 and R2 FACs and the Pedersen conductivity. Therefore, particle precipitation from the ring current-plasmapause and the topside electron temperature also affect the intensity of SAPS.

In this study, we use measurements of the Defense Meteorological Satellite Program (DMSP) satellites to investigate the characteristics of electron temperature in the topside subauroral ionosphere during the magnetic storm on 17 March 2015, the St. Patrick's day storm. A prominent feature of this storm is its long recovery phase. Many previous studies have analyzed the ionospheric response to this storm (Zhang et al., 2017 and references therein), but the behavior of the ionospheric electron temperature, especially during the long recovery phase of the storm, is unknown. We show for the first time that the topside electron temperature in the subauroral ionosphere was enhanced continuously for 8 days. The mechanism for this long-lasting ionospheric heating process will also be discussed.

2. Observations

We first present the solar wind and geomagnetic conditions during this magnetic storm. Figure 1 shows the solar radio flux at 10.7 cm (1 sfu = 10^{-22} W m^{-2} Hz^{-1}), the solar wind speed, the B_y and B_z components of the interplanetary magnetic field (IMF), the Dst index, and the AE index on 15–25 March 2015. Note that the date in the horizontal axis runs from right to left for an easy comparison with the DMSP data. The onset of the magnetic storm was at 06:00 UT on 17 March. The minimum Dst reached −223 nT at 22:00 UT on 17 March, and Dst became positive at 12:00 UT on 25 March. The recovery phase of the magnetic storm lasted for ∼7.5 days. Such a long recovery phase was determined by the solar wind conditions. The solar radio flux was largely unchanged for the first 5 days since the storm onset and had some small increases during the later recovery phase. The solar wind speed suddenly increased at the storm onset and remained elevated throughout the entire main and recovery phases, indicating that this storm was a high-speed solar wind stream event. The IMF B_y and B_z components had large variations during the storm main phase and fluctuated between positive and negative during the recovery phase. The insets in Figures 1c and 1d show the detailed variations of the B_y and B_z components on 1 day (20 March); B_y and B_z fluctuated between −7 and 7 nT. The AE index increased to ∼2,000 nT during the storm main phase and showed irregular enhancements (up to 1,000 nT) during the recovery phase. The high-speed solar wind streams and fluctuating B_y and B_z continuously drove the magnetic activity during the entire process of the

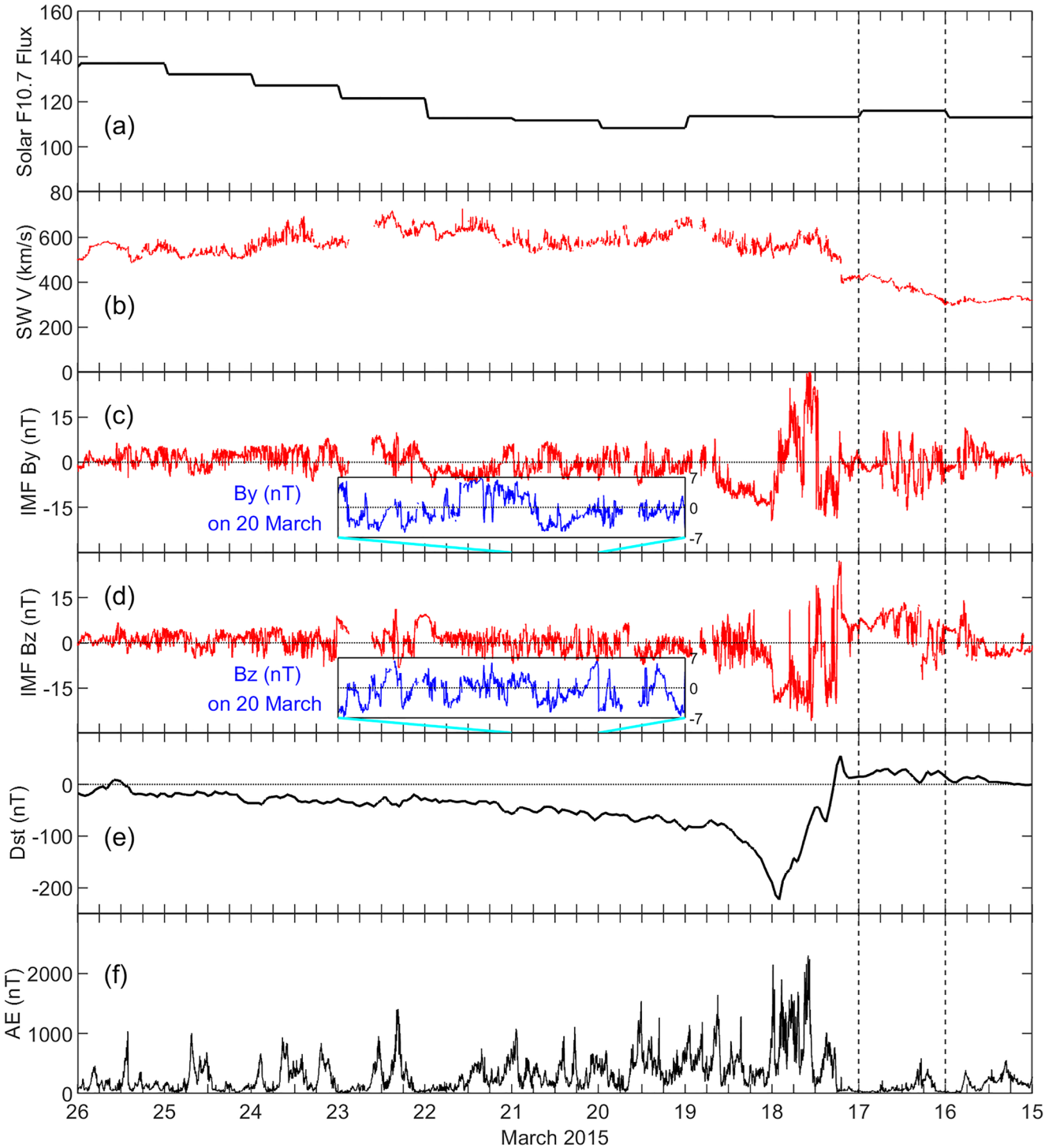

Figure 1. Solar radio flux at 10.7 cm (sfu = 10^{-22} W m^{-2} Hz^{-1}), solar wind velocity, interplanetary magnetic field (IMF) B_y and B_z components, Dst index, and AE index on 15–25 March 2015. The two vertical lines are used to denote a reference day on 16 March. The date in the horizontal axis runs from right to left.

storm. On 16 March, the IMF B_z was mostly positive, Dst was positive, and AE was small; this day is used as a quiet-time reference day.

The ion density (N_i) and electron temperature (T_e) data used in this study are from measurements of the DMSP F15, F16, and F19 satellites. The uncertainty in DMSP measurements of N_i and T_e is within 10% (Rich, 1994;

Sultan & Rich, 2001). The DMSP satellites are in sun-synchronous polar orbits at an altitude of ~840 km, with an orbital period of ~100 min. The DMSP satellites fly from the southern to northern hemisphere in the dusk sector and from the northern to southern hemisphere in the dawn sector. In this study, we focus on the ionospheric phenomena in the post-midnight and dawn sector. The DMSP F15, F16, and F19 satellites crossed the equator in the midnight-dawn sector at ~02:45 LT, ~04:30 LT, and ~06:30 LT, respectively.

Figure 2 presents N_i and T_e measured by the F16 satellite on 15–25 March 2015. The magenta dots denote the equatorward boundary of the auroral zone that is determined from the DMSP measurements of electron energy flux and referred to as the Auroral Boundary Index (Gussenhoven et al., 1983; Hardy et al., 1985; Huang et al., 2021). As mentioned above, the magnetic activity was weak on 16 March, and the measurements on this day are used as a reference. Figure 2b shows the difference ion density ($\Delta\log_{10}N_i$) between N_i during the storm days and N_i on 16 March (the quiet-time reference day). $\Delta\log_{10}N_i$ is defined to be $\log_{10}N_{i,\text{ measured}}$ - $\log_{10}N_{i,\text{ reference}}$, and this actually represents the ratio $\log_{10}(N_{i,\text{ measured}}/N_{i,\text{ reference}})$. A change of unity in $\Delta\log_{10}N_i$ represents a change of an order of magnitude in N_i. The N_i values at the same UTs on the storm days and the reference days are used to calculate the difference N_i. As can be seen in Figure 2b, N_i had large increases and decreases during the first 2 days of the magnetic storm, which may be caused by penetration and disturbance dynamo electric fields and thermospheric composition changes. The changes in N_i became smaller during the late stage of the storm recovery phase.

Figures 2c and 2d show T_e and difference electron temperature (ΔT_e). ΔT_e is defined to be the difference between the storm-time T_e and the T_e on the reference day, representing the net change of T_e caused by the magnetic storm. T_e was high at subauroral latitudes and low at middle and low latitudes. The most important feature is that T_e at subauroral latitudes, equatorward of the auroral boundary, was continuously enhanced for 8 days during the magnetic storm, from the onset of the storm to the end of the recovery phase. The temperature increase reached 2000 K or higher.

At subauroral latitudes, the region of enhanced T_e overlaps the region of decreased N_i, which represents the situation in the midlatitude trough and will be further discussed later. In contrast, at middle and low latitudes, the changes in T_e were small. In the ionosphere, changes in T_e are typically correlated with changes in N_i through the cooling effect. The electron cooling rate through electron–ion Coulomb collision is proportional to the square of plasma density (Schunk & Nagy, 1978), so an ion density enhancement is often related to an electron temperature decrease and vice versa. However, the electron cooling rate through the Coulomb collision process becomes small when the plasma density is low enough. Zhang, Holt, et al. (2004) examined ionospheric plasma temperature data measured by an incoherent scatter radar and found that a N_e (electron density, same as N_i) threshold exists and turns on and off its effects on T_e. Night-time T_e at middle and low latitudes is controlled mainly by the thermal balance between neutrals, ions, and electrons and does not depend much on N_e when N_e is low. In our case, the measurements in Figure 2 were made in the post-midnight sector, and the small changes in T_e at middle and low latitudes can be explained by low cooling rate because of the low ion density at night.

It can be seen in Figure 2c that higher T_e in the northern hemisphere extended to middle latitudes around 09:00 UT every day. In order to show the details of the storm-time variations, the N_i and T_e data are plotted over a range of 2 days, two quiet days in Figures 3a and 3b and two storm days in Figures 3c and 3d. The low-density region just equatorward of the auroral boundary in both hemispheres in Figures 3a and 3c represents the "main ionospheric trough" or "midlatitude trough" (Moffett & Quegan, 1983; Prölss, 2007). An interesting phenomenon is that N_i is enhanced equatorward of the trough during both the quiet days and the storm days, compared with the N_i at low latitudes. Therefore, the enhanced N_i bands equatorward of the midlatitude trough is a persistent ionospheric phenomenon, rather than a storm effect. Although Figure 3 is plotted in geographic latitude, the enhanced N_i bands are 30°–40° from the magnetic equator. In other words, the enhanced N_i bands are located at 30°–40° magnetic latitude. The physical mechanism for the formation of the enhanced N_i bands will be discussed later.

Figures 3b and 3d show that the extension of higher electron temperature to middle latitudes in the northern hemisphere occurs over North Atlantic Ocean. In this region, the magnetic field has large west declination (https://www.ngdc.noaa.gov/), and the magnetic field lines tilt toward western longitudes in the northern hemisphere and toward eastern longitudes in the southern hemisphere. The DMSP F16 measurements in the northern hemisphere were made at ~04:30 LT, but its magnetic conjugate point in the southern hemisphere was at later local times in the morning sector. Photoelectrons in the morning sector cause higher electron temperature in the southern

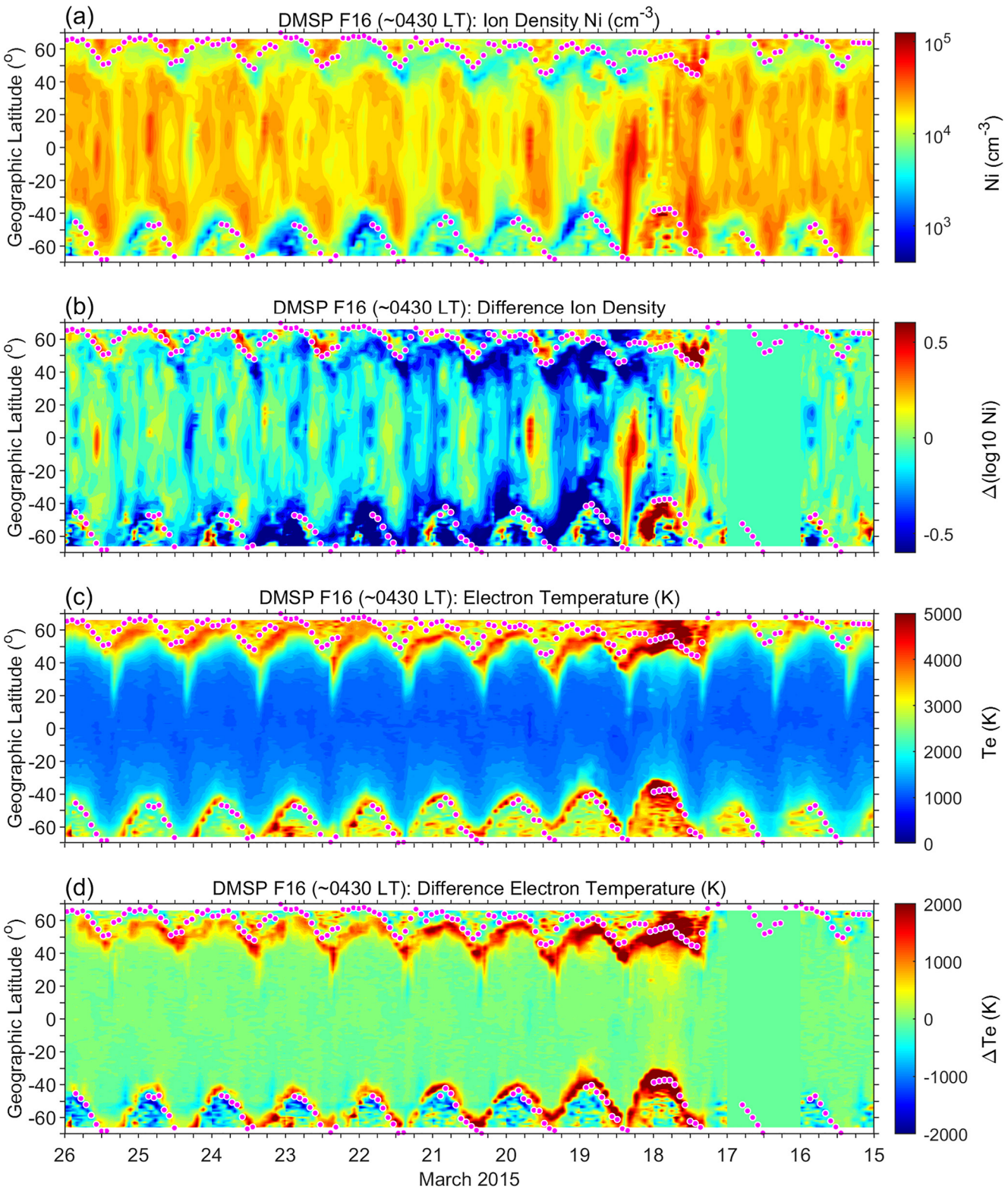

Figure 2. Ion density, difference ion density, electron temperature, and difference electron temperature measured by the DMSP F16 satellite in the post-midnight sector on 15–25 March 2015.

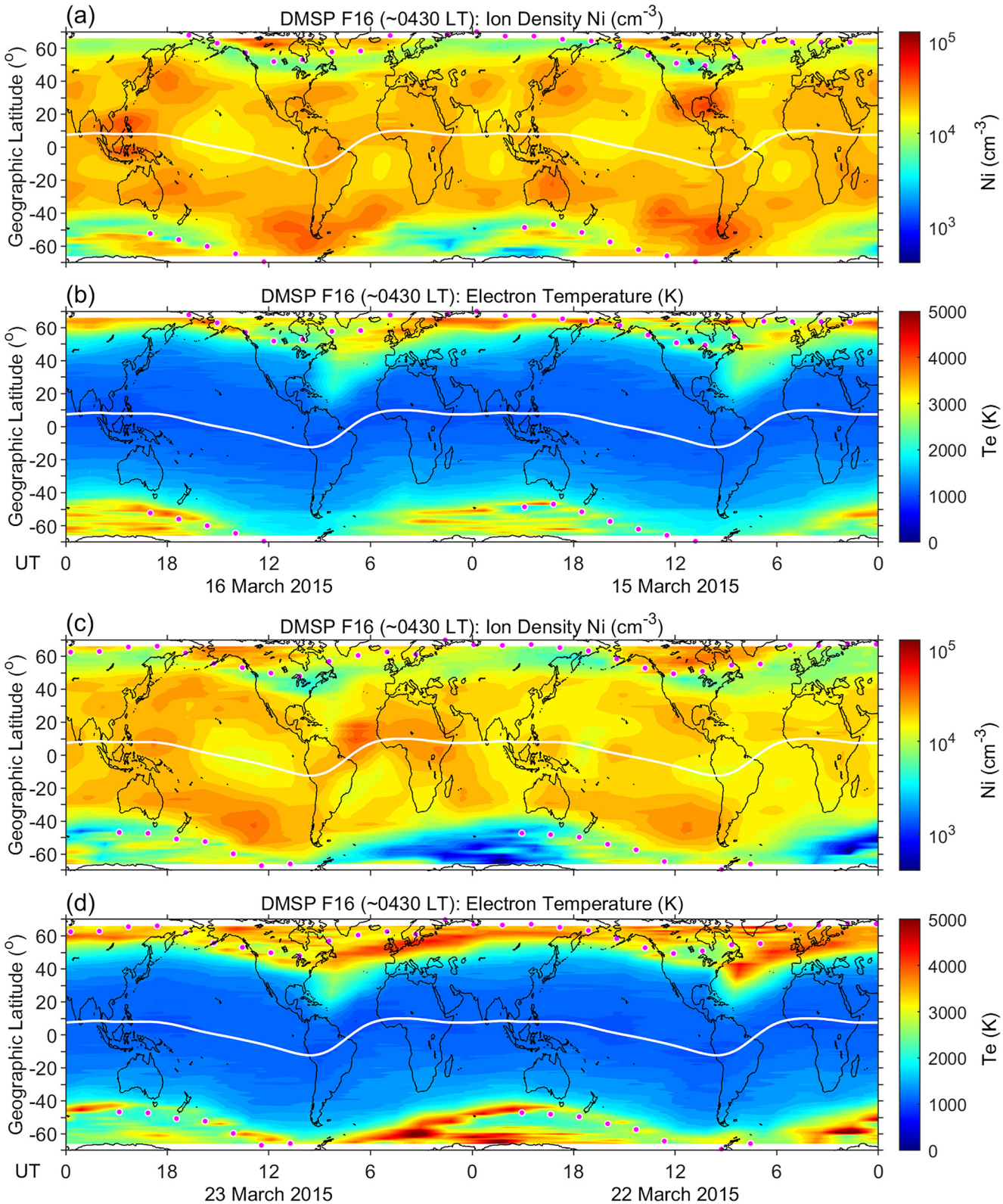

Figure 3. (a)–(b) Ion density and electron temperature measured by the DMSP F16 satellite in the post-midnight sector on 15–16 March 2015. (c)–(d) Ion density and electron temperature on 22–23 March 2015. The white curve denotes the dip equator.

hemisphere, and these electrons can move along the magnetic field lines to the nighttime northern hemisphere and cause higher temperature. The occurrence of higher electron temperature over North Atlantic Ocean measured by the DMSP F16 satellite at 04:30 LT can be explained by this mechanism.

Besides the F16 satellite, the DMSP F15 satellite also made measurements of N_i and T_e in the post-midnight sector. The measurements of F15, shown in Figure 4, were made near 02:45 LT. In this case, the F15 measurements had many data gaps on 15 March 2015, so the F15 data on this day is not plotted. During the magnetic storm, N_i was largely decreased, and T_e was enhanced at subauroral latitudes but had small changes at middle and low latitudes. The variations of N_i and T_e measured by F15 were very similar to those measured by F16, providing a cross validation of the measurements by the two satellites.

The F16 measurements in Figure 3 show the occurrence of enhanced N_i bands equatorward of the midlatitude trough. This feature was also measured by F15, as presented in Figure 5. One difference in T_e between the F15 data and the F16 data is that the enhanced T_e measured by F15 existed only at subauroral latitude but did not extend to middle latitudes. This is because the F15 measurements were made at ~02:45 LT, earlier than the local time of the F16 measurements. At 02:45 LT, the magnetic conjugate points in the two hemispheres are both within night time, and T_e at those locations are not affected by photoelectrons.

Another satellite, the DMSP F19 satellite, made measurements near dawn (~06:30 LT) in this case, and the F19 data are depicted in Figure 6. At this local time, N_i increased between 12:00 UT on 17 March and 12:00 UT on 18 March and then decreased, especially in the southern hemisphere during the following days. The T_e data show some unique features in this local time sector. As can be seen in Figure 6c, T_e was large at low latitudes during the quiet days (15–16 March 2015). T_e at low latitudes near sunrise can be a few hundred Kelvin higher than that at night. This phenomenon has been observed for a long time and is termed the morning overshoot (e.g., Evans, 1965; Oyama et al., 1996; Stolle et al., 2011). The ionospheric electron temperature on the dayside is determined by the balance among heating by photoelectrons, cooling by collision with the ions and neutrals, and thermal heat conduction. The heating rate is approximately linear with respect to the plasma density while the cooling rate is quadratic with respect to the plasma density. At sunrise, the plasma density is low, but the electron heating from photoelectrons occurs promptly, resulting in higher temperature in the ambient electrons and the morning overshoot.

We are interested in the storm-time changes in T_e. As can be seen in Figure 6c, T_e was high at most latitudes but became relatively low around −40° latitude. A sharp boundary (or decrease) in T_e occurred at 20-30° latitude in the southern hemisphere, and this boundary appeared to move gradually toward higher southern latitudes. Figure 6d shows ΔT_e during the magnetic storm. T_e enhancements occurred primarily at middle and subauroral latitudes in the southern hemisphere.

In order to understand the occurrence of the T_e boundary in the southern hemisphere and its movement toward higher latitudes, $\Delta \log_{10} N_i$, ΔT_e, and T_e during the first five days of the storm are plotted in Figure 7; the continents and the dip equator are depicted to show the offset between the geographic and geomagnetic equators and its relationship with the locations of the midlatitude troughs and corresponding T_e enhancements. N_i increased during the first 1.5 days and then decreased most times during the following days. In particular, decreases in N_i were large at southern subauroral latitudes, representing a deepened trough in the southern hemisphere. The changes in T_e were negatively correlated with the changes in N_i. This negative correlation between N_i and T_e occurred in the sunlit ionosphere and is consistent with the enhanced cooling effect when the ambient plasma density is high (Schunk & Nagy, 1978). When the midlatitude trough and related T_e changes moved toward higher latitudes in the southern hemisphere, the boundary in T_e also moved gradually toward higher latitudes. The midlatitude trough occurs, in general, at night (Moffett & Quegan, 1983). The occurrence of the trough in the southern hemisphere during daytime will be discussed later.

It can also be seen in Figures 7b and 7c that quasi-periodic enhancements occurred in T_e. These T_e enhancements had a quasi-period of ~6 hr and were well correlated with corresponding decreases in N_i. Similar enhancements in T_e also occurred during the quiet days and can be seen in Figure 6. These quasi-periodic enhancements in T_e are the well-known wave-4 longitudinal structures (e.g., Immel et al., 2006). The wave-4 structures appeared to have been enhanced and to extend to middle latitudes during the magnetic storm.

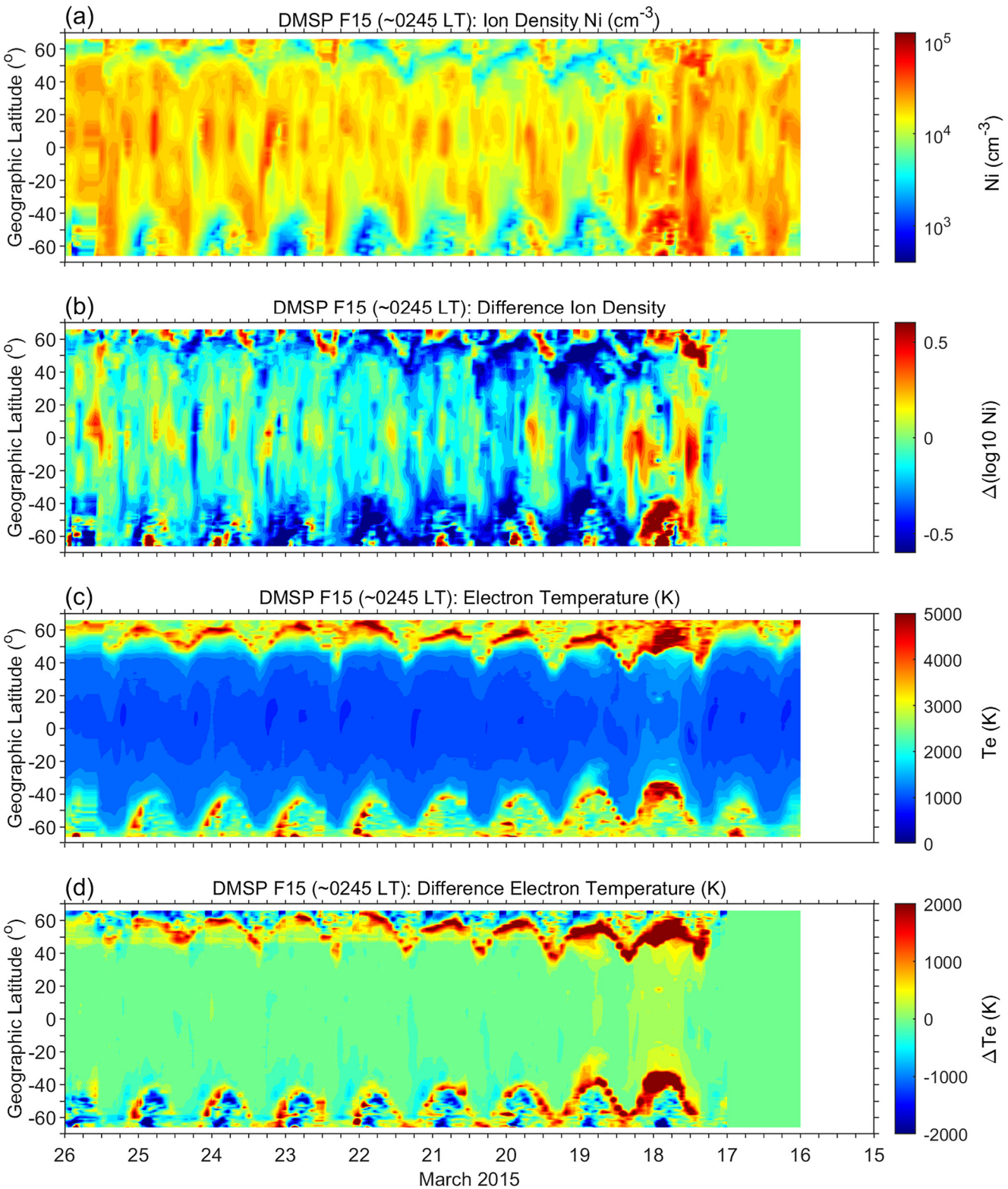

Figure 4. Ion density, difference ion density, electron temperature, and difference electron temperature measured by the DMSP F15 satellite in the post-midnight sector on 15–25 March 2015.

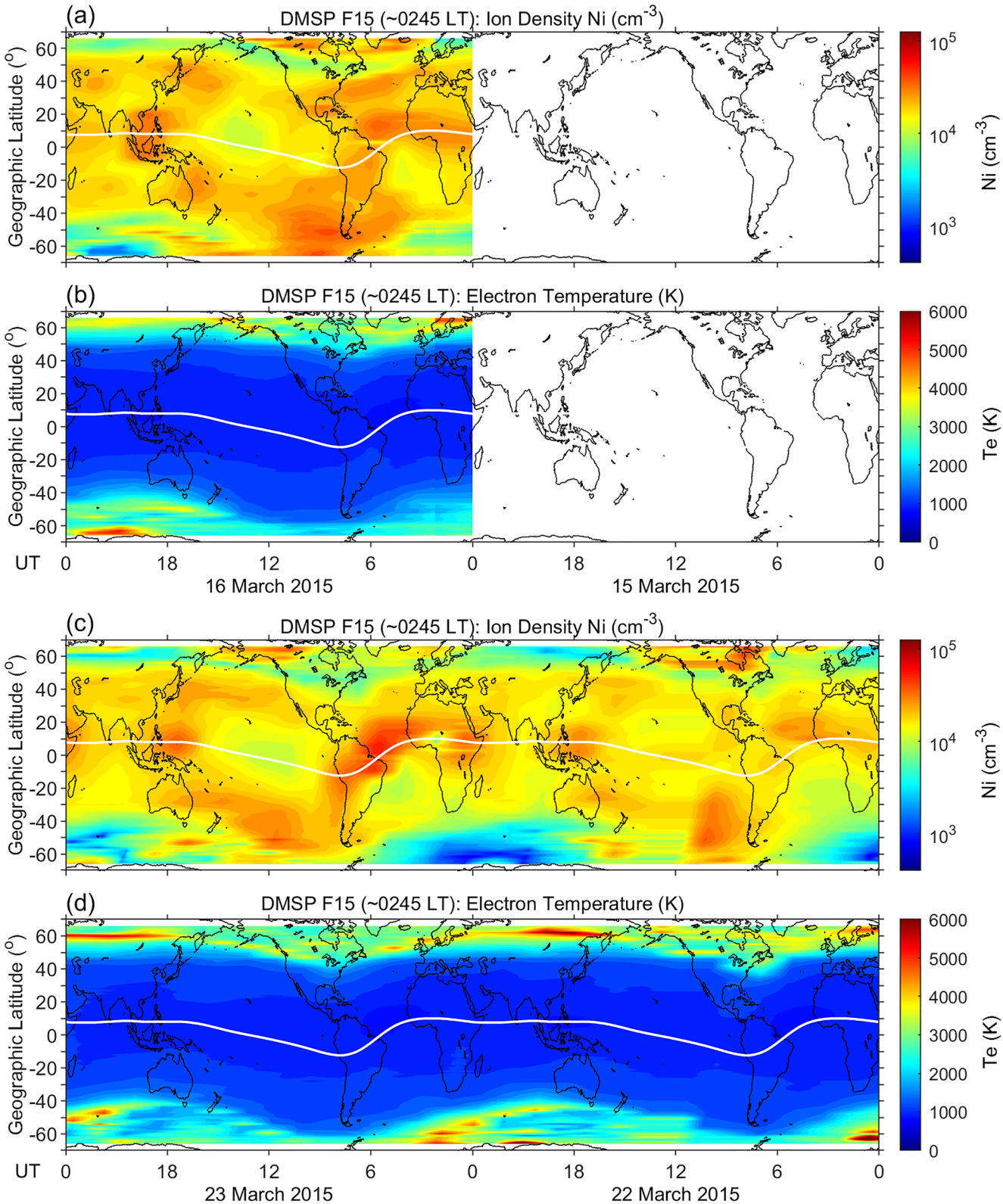

Figure 5. (a)–(b) Ion density and electron temperature measured by the DMSP F15 satellite in the post-midnight sector on 15–16 March 2015. (c)–(d) Ion density and electron temperature on 22–23 March 2015.

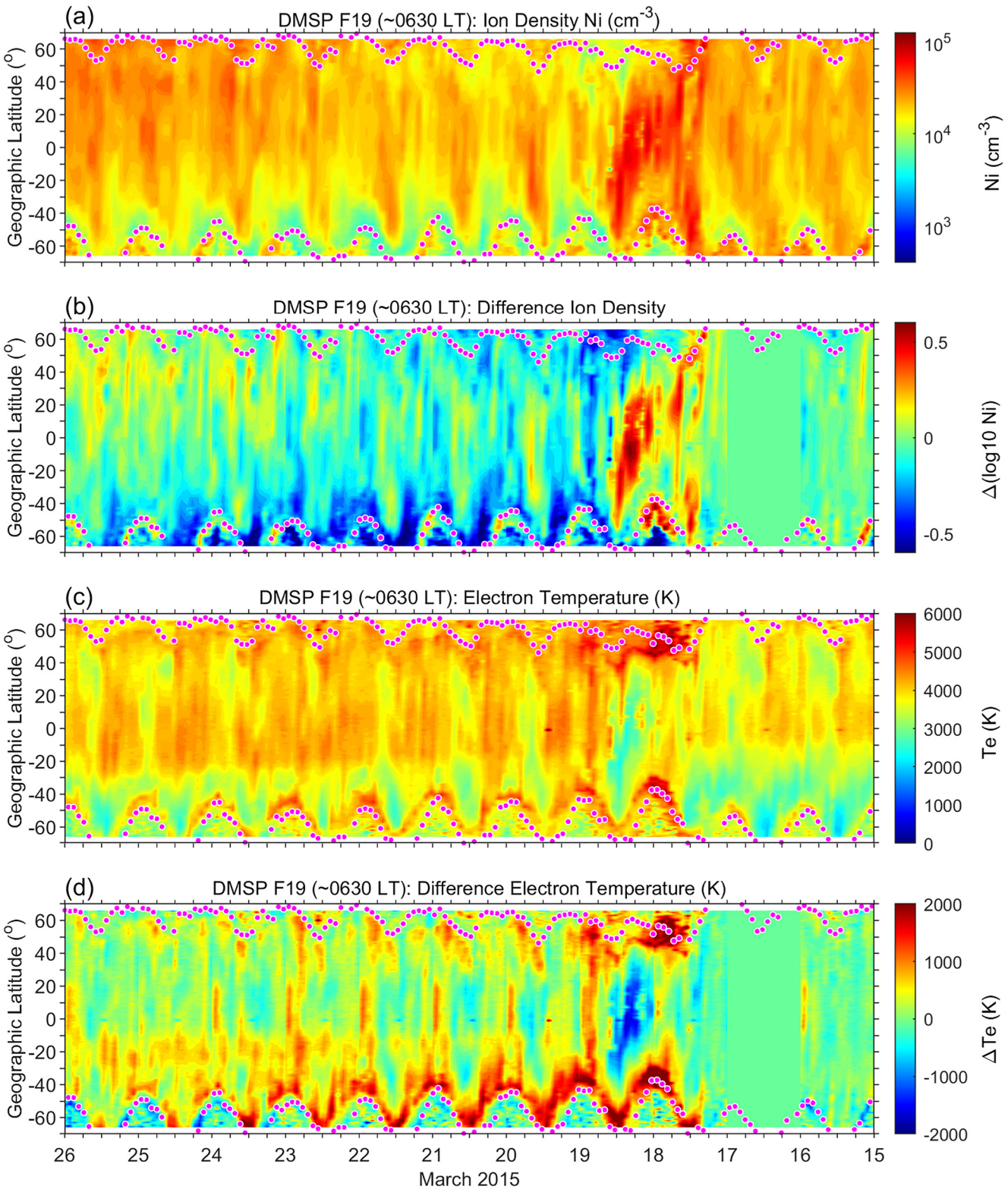

Figure 6. Ion density, difference ion density, electron temperature, and difference electron temperature measured by the DMSP F19 satellite near dawn on 15–25 March 2015.

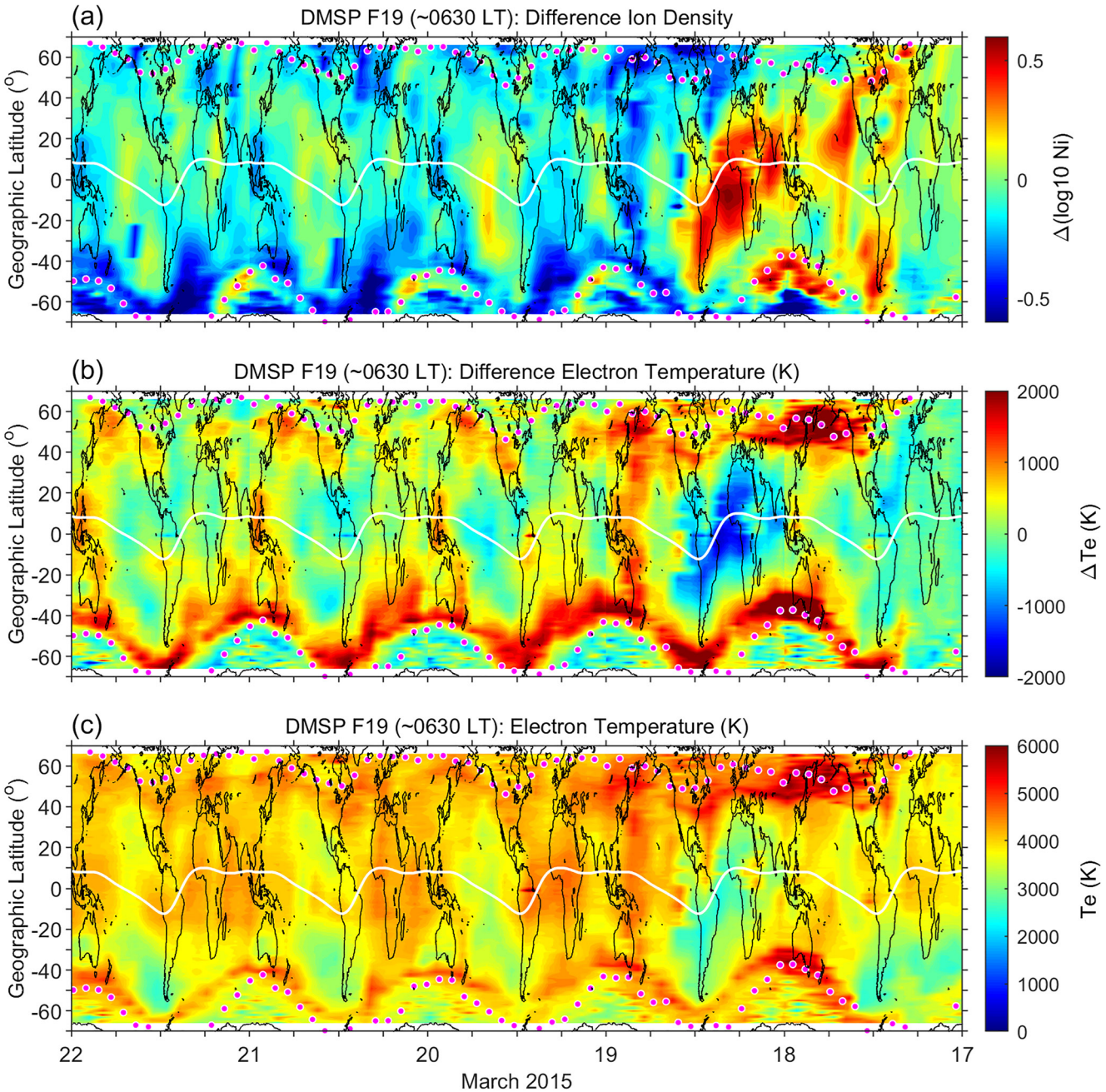

Figure 7. (a) Difference ion density, (b) difference electron temperature, and (c) electron temperature measured by the DMSP F19 satellite near dawn on 17–21 March 2015.

The above figures all show enhancements of T_e at subauroral latitudes during the storm times. We now calculate the quantitative changes of T_e. In Figure 8a, the blue and red curves represent the T_e data along the orbit of the DMSP F16 satellite on 16 and 18 March 2015, respectively. The UTs during the two orbits were very close, implying that the measurements on the 2 days were made at about the same longitudes. The difference in T_e between the 2 days was caused by the magnetic storm but not by longitudinal variations. On the quiet day of 16 March, maximum T_e occurred at ~±60° magnetic latitude and was ~4,000 K. On the storm day of 18 March, maximum T_e occurred at ~±48° magnetic latitude and reached ~5,000 K.

We use two different methods to calculate the changes of T_e. The first method is to calculate the storm time change of the maximum T_e. In Figure 8a, the maximum T_e at −60° magnetic latitude in the southern hemisphere on 16 March is marked with $T_{e(\text{max, quiet})}$, and the maximum T_e at −47.5° on 18 March is marked with $T_{e(\text{max, storm})}$,

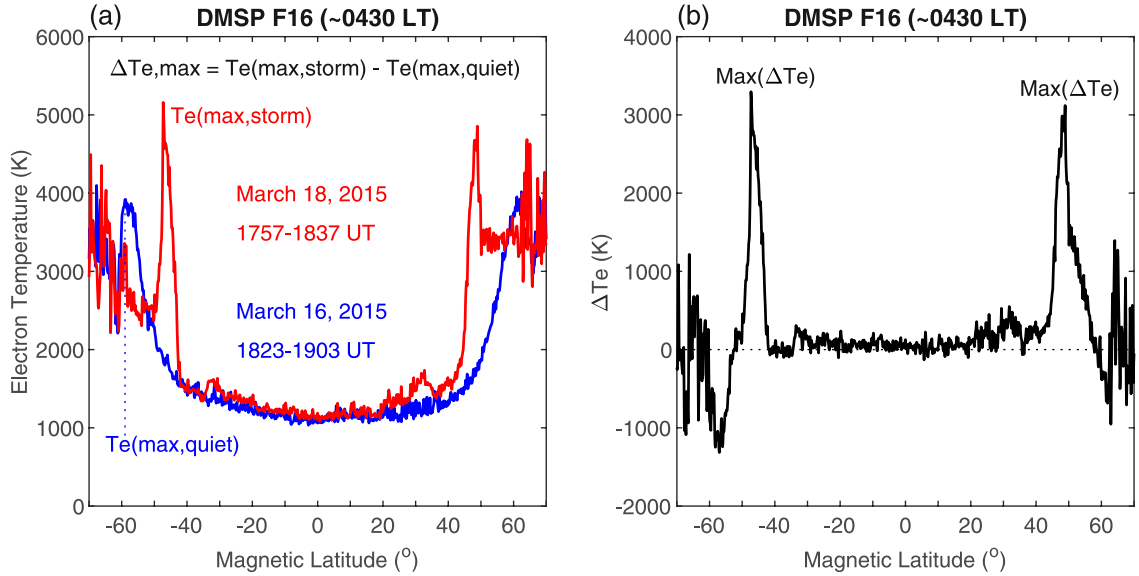

Figure 8. (a) Example of electron temperature measured by the DMSP F16 satellite at ~04:30 LT during two orbits on 16 and 18 March 2015. (b) Difference electron temperature between the two DMSP orbits on 16 and 18 March 2015.

respectively. The storm-time change of the maximum T_e is defined to be $\Delta T_{e,\max} = T_{e(\max,\ \text{storm})} - T_{e(\max,\ \text{quiet})}$. The storm-time change of T_e in the northern hemisphere is defined similarly. Note that in this method, the quiet-time maximum T_e and the storm-time maximum T_e occurred at different latitudes.

A second method to calculate the storm-time change of T_e is shown in Figure 8b. In this method, the difference between the storm-time T_e and the T_e on the reference day, denoted as ΔT_e, is calculated first, and the maximum values of ΔT_e, denoted as $\max(\Delta T_e)$, in the northern and southern hemispheres are then determined. The $\max(\Delta T_e)$ represents the maximum enhancement of T_e at the storm-time subauroral latitudes.

The results of the storm-time changes of T_e based on the two methods are presented in Figure 9. Figures 9b and 9c show the storm-time change of the maximum T_e, $\Delta T_{e,\max}$ calculated with the first method, measured by the DMSP F15 and F16 satellites. The results show that the storm-time maximum T_e was 1,000–2,000 K higher than the quiet-time maximum T_e for eight days, from the onset of the storm to the end of the storm recovery phase. Figures 9d and 9e show the maximum value of the difference T_e, $\max(\Delta T_e)$ calculated with the second method, indicating that the maximum T_e at storm-time subauroral latitudes increased by 1,000–4,000 K for 8 days.

Figure 9f shows the maximum T_e at subauroral latitudes measured by the DMSP F15 and F16 satellites in the northern hemisphere. It can be seen that the maximum T_e during the storm days was higher than the maximum T_e on the quiet day of 16 March, consistent with the results in Figures 9b–9e. An interesting feature in Figure 9f is that the maximum T_e showed a strong daily variations during the storm days, especially in the measurements of F15 (the blue curve). The largest maximum T_e occurred between 18:00 and 24:00 UT every day.

3. Discussion

The observations presented in the previous section show enhancement of T_e at subauroral latitudes during the magnetic storm on 17–25 March 2015. Previous studies reported storm-time T_e enhancement at subauroral latitudes and the relationship between T_e enhancement and geomagnetic activity (e.g., Brace et al., 1974, 1988; Kozyra et al., 1986; Prölss, 2006), and it was suggested that energy is transferred from the hot ring current ions to the cold plasmaspheric particles through Coulomb collisions and that the thermal electron precipitation from the plasmapause region along magnetic field lines causes T_e enhancement in the subauroral ionosphere. In our case, the T_e enhancement also occurred at subauroral latitudes, and our observations are consistent with previous results.

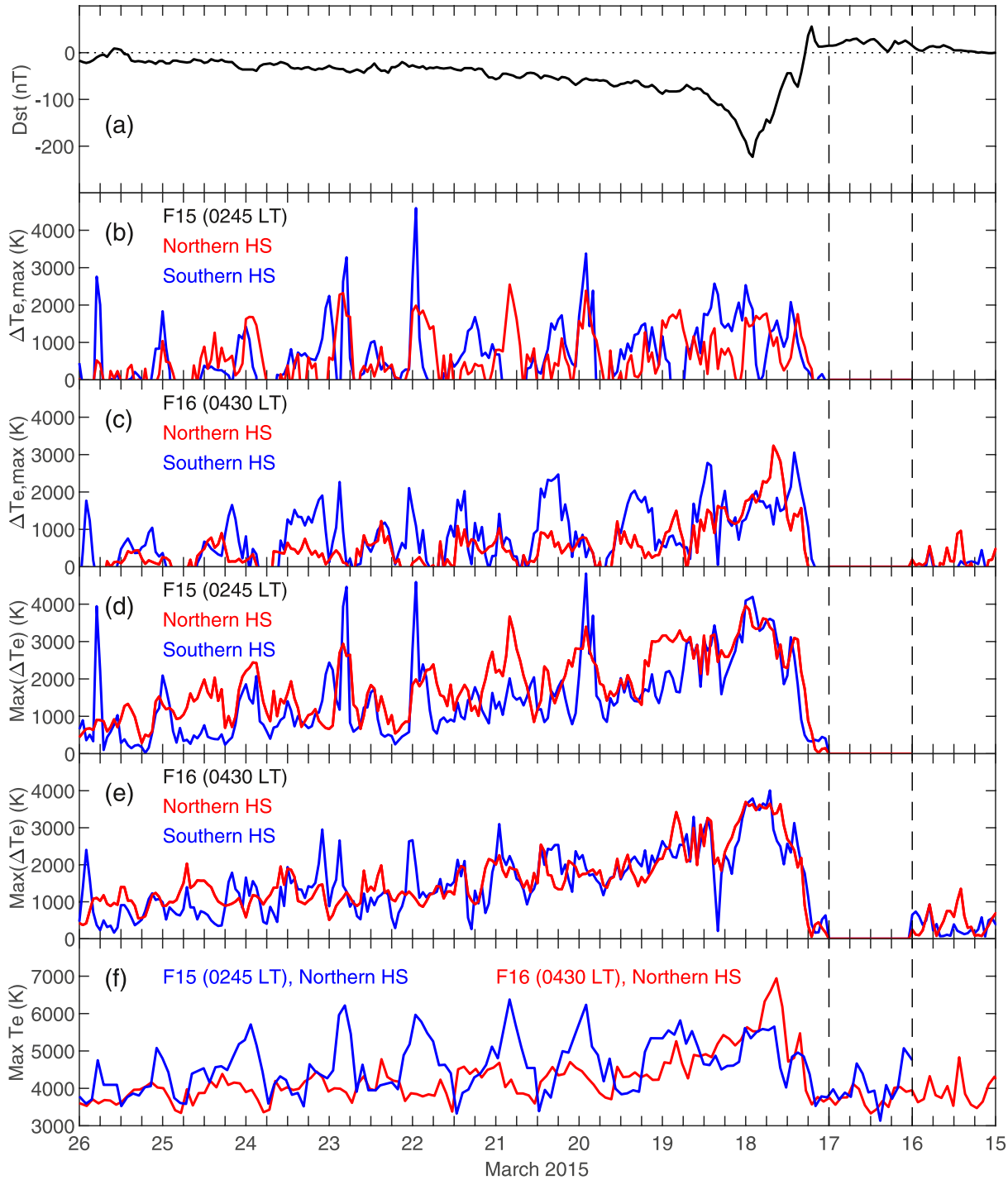

Figure 9. The Dst index and the electron temperature measured by the DMSP F15 and F16 satellites. See text for the definitions of the difference electron temperatures and the maximum electron temperature.

The unusual feature in our case is that the T_e enhancement lasted for 8 days, indicating that energy was continuously transferred from the ring current-plasmasphere to the ionosphere for this long period if the energy source for ionospheric T_e increases is assumed to be inner magnetospheric heat flux or soft particle precipitation from the plasmapause. The magnetic storm in the current study indeed had some peculiar characteristics. As can be seen in Figure 1, the solar wind velocity was as high as 600 km s^{-1} for 8 days, and the IMF B_y and B_z were fluctuating in the range of ±7 nT during the long recovery phase of the storm. A solar wind-magnetosphere coupling

function is defined by Newell et al. (2007) as $d\Phi_{MP}/dt = v^{4/3} B_T^{2/3} \sin^{8/3}(\theta/2)$, where v is the solar wind velocity, B_T is the IMF magnitude in the plane transverse to the solar wind velocity, and θ is the IMF clock angle. This coupling function represents the magnetic flux merging rate in the dayside magnetopause. Both large solar wind velocity (v) and southward IMF ($\theta > 90°$) increase energy transfer from the solar wind to the magnetosphere, leading to enhancements of magnetic activity and the ring current, as well as the subauroral electron temperature. The energy transfer processes, including energy transfer from the solar wind to the magnetosphere through high-speed solar wind stream and fluctuating IMF B_y and B_z, energetic particle injections from the magnetotail into the ring current, energy transfer from the ring current to the plasmasphere, and particle precipitation from the plasmapause to the subauroral ionosphere, continued occurring throughout the entire period of the magnetic storm. Although Dst became small during the later recovery phase of the storm, the AE index remained at high level, from a few hundred nT to ∼1,000 nT, indicating continuous energy injection into the ionosphere. The long-lasting T_e enhancement in this case is the consequence of the energy transfer processes among the solar wind, magnetosphere, ring current, plasmasphere, and ionosphere. An important implication of the observations is that the electron temperature in the subauroral ionosphere can be significantly enhanced under fluctuating IMF conditions even if the storm activity, represented by the Dst index, is not very strong.

Figure 9f shows that the maximum T_e at subauroral latitudes measured by the DMSP F15 satellite, depicted by the blue curve, had large daily variations. We suggest that these UT variations of T_e actually represent variations with latitude. As can be seen in Figures 5c and 5d, the enhanced T_e band overlaps with the midlatitude trough, and the northern trough is located at the highest geographic latitude over Asia (around 18:00 UT) but shifts to the lowest geographic latitudes near the east coast of North America (around 07:00 UT) because of the offset between the magnetic and geographic latitudes. Higher T_e in the trough region occurs at higher latitudes and is related to lower N_i. Thermospheric O/N_2 density ratio is lower at higher latitudes than that at lower latitudes (Zhang, Paxton, et al., 2004), which may cause lower N_i at higher latitudes and higher N_i at lower latitudes and further affect T_e through the cooling process. The daily variation of the maximum T_e can be explained by the latitudinal variation of O/N_2 ratio and the latitudinal shift of the trough at a fixed local time along the DMSP orbit.

The daily variations of the maximum T_e measured by the DMSP F16 satellite, depicted by the red curve in Figure 9f, are much smaller than those measured by F15. The measurements of F15 and F16 were made at ∼02:45 and ∼04:30 LT, respectively. The N_i and T_e in the northern regions with westward magnetic declination at 04:30 LT may be affected by photoelectrons in the sunlit conjugate southern ionosphere. However, it is not certain how strong such influence from the conjugate ionosphere could be.

Equatorward of the midlatitude trough, enhanced N_i bands were observed in both the southern and northern hemispheres. The enhanced N_i bands occurred during both the quiet days and the storm time and are located at 30-40° magnetic latitude. Previous studies by Lee et al. (2011) and Zhong et al. (2019) showed the occurrence of similar higher ion density or TEC values equatorward of the midlatitude trough in the post-midnight sector. We suggest that several processes may be responsible for the occurrence of the enhanced N_i bands. (a) Outflows from the daytime ionosphere increases plasmaspheric particle density, and plasmaspheric particles flow down along field lines to the midlatitude ionosphere at night and lead to enhanced N_i at middle latitudes. (b) Energetic particle precipitation from the inner radiation belt was observed at low latitude zones ($L = 1.6$–1.8) (Nagata et al., 1988 and references therein), and the corresponding invariant latitude range is around 40°. The precipitation protons and electrons may cause enhanced ionization in the nightside ionosphere. (c) Equatorial plasma drifts are typically downward in the post-midnight sector (Fejer et al., 2008), causing low plasma density in the equatorial and low-latitude topside ionosphere and the occurrence of relatively high plasma density at middle latitudes.

The storm-time T_e near dawn shows very different features from the T_e at night. As can be seen in Figure 6, enhanced T_e gradually expanded toward higher latitudes in the southern hemisphere. This variation in T_e is related to the variation of the midlatitude trough, as discussed in the previous section. Then the question is why the midlatitude trough occurs only in the southern hemisphere but not in the northern hemisphere near dawn. Mallis and Essex (1993) studied the characteristics of the midlatitude trough near Macquarie Island (geographic coordinates 54.5° S, 154.95° E, geomagnetic coordinates 64.5° S, 177.67° E, $L = 5.38$) and found that the trough occurs more frequently during daytime than during nighttime at Equinox. The daytime occurrence of the midlatitude trough at this location may be related to the existence of the south magnetic pole at very low geographic latitude near the longitude of Macquarie Island.

In our case, the midlatitude trough near dawn was deep and occurred at all longitudes in the southern hemisphere, and the corresponding T_e enhancement was large, as shown in Figures 6 and 7. This is consistent with the observation of Mallis and Essex (1993). In the northern hemisphere, the existence of the trough and the corresponding T_e enhancement can also be seen in Figure 7, especially in the ΔT_e data, and the enhanced T_e occurred largely over North America and North Pacific Ocean where the magnetic declination is westward. It appears that the storm-time enhanced T_e and midlatitude trough near dawn show large interhemispheric asymmetry and strong dependence on the magnetic declination.

A recent study of Huang et al. (2021) shows that enhanced eastward ion drifts occur at subauroral latitudes in the dawn sector during intense magnetic storms. The storm enhanced eastward ion drifts are termed dawnside SAPS. In the present case, dawnside SAPS also occurred and coincided with the T_e enhancement (the SAPS data are not presented). The primary energy source of the subauroral T_e enhancement is mostly likely to be soft electron precipitation from the ring current-plasmapause region, but the strong eastward plasma drifts (the dawnside SAPS) could also have some effects on the T_e enhancement.

In this study, we focus on the enhancement of T_e at subauroral latitudes measured by the DMSP F15, F16, and F19 satellites in the predawn sector. The T_e enhancement in the predawn sector was caused primarily by soft particle precipitation from the ring current-plasmapause region because the effects of photoelectrons can be excluded. The DMSP F15, F16, and F19 satellites in this case flew over the ionosphere near 14:45, 16:30, and 18:30 LT in the afternoon-dusk sector, respectively. T_e in the sunlit hemisphere, including the subauroral regions, is controlled by photoelectron heating (Schunk & Nagy, 1978). Furthermore, particle precipitation from the ring current occurs primarily on the nightside and becomes relatively weak on the dayside (e.g., Jordanova et al., 2001). The dayside particle precipitation does not cause significant change in the ionospheric T_e because of high plasma density. Thus T_e measured by the DMSP satellites in the afternoon sector was largely not affected by the ring current activity and did not show the long-lasting enhancement during the recovery phase of this magnetic storm.

4. Summary

This study investigates the subauroral electron temperature enhancement and the cause for the temperature enhancement measured by the DMSP satellites during the magnetic storm on 17–25 March 2015. The results are summarized as follows.

The topside F-region electron temperature at subauroral latitudes in the post-midnight sector was continuously enhanced for 8 days from the storm onset to the end of the recovery phase. The storm-time maximum electron temperature was higher than the corresponding quiet-time maximum temperature by 1,000–4,000 K and occurred at lower latitudes. The long-lasting enhancement of the subauroral electron temperature is explained as the consequence of continuous particle precipitation from the ring current-plasmapause region. The solar wind velocity remained high for 8 days during the magnetic storm, and the IMF By and Bz were fluctuating. The fluctuating IMF Bz turns on/off energy transfer from the solar wind to the magnetosphere and the ring current. The slow recovery of the ring current leads to continuous particle precipitation into the subauroral ionosphere and the continuous enhancement in the subauroral electron temperature.

The electron temperature increases were quite symmetric between the southern and northern hemispheres in the post-midnight sector. In contrast, the electron temperature enhancement near dawn showed strong interhemispheric asymmetry, and the electron temperature enhancement in the southern hemisphere was much larger than that in the northern hemisphere. This interhemispheric asymmetry in electron temperature enhancement near dawn may be related to the magnetic declination and the offset between the magnetic and geographic latitudes.

The maximum electron temperature at subauroral latitudes in the post-midnight sector showed large daily variations. Higher electron temperature was observed when the subauroral region was at higher geographic latitudes. The variations of the maximum electron temperature may be related to thermospheric O/N2 ratio and its effect on the ion density.

Enhanced ion density bands occurred at 30-40° magnetic latitudes, equatorward of the midlatitude trough, in the post-midnight sector during both quiet times and storm times. The enhanced ion density bands may be caused by plasma particle precipitation from the plasmasphere and inner radiation belt and westward electric fields in the nighttime equatorial ionosphere.

Disclaimer

The views expressed are those of the authors and do not reflect the official guidance or position of the United States Government, the Department of Defense or of the United States Air Force. Statement from DoD: The appearance of external hyperlinks does not constitute endorsement by the United States Department of Defense (DoD) of the linked websites, or the information, products, or services contained therein. The DoD does not exercise any editorial, security, or other control over the information you may find at these locations.

Data Availability Statement

The authors acknowledge the CEDAR madrigal database (http://cedar.openmadrigal.org/) for providing DMSP thermal plasma particle data, and the Space Physics Data Facility at Goddard Space Flight Center (https://omniweb.gsfc.nasa.gov/) for providing solar wind, Dst, and AE data.

Acknowledgments
Work at the Air Force Research Laboratory was supported by NASA grants 80HQTR20T0015, 80HQTR20T0016, and NNH22OB17A. DL and WW are supported in part by NASA grants 80NSSC17K0013, 80NSSC19K0835, 80NSSC20K0601, and 80NSSC20K0356, and NSF CEDAR grant AGS-2033843. QW is supported by NASA grants 80NSSC20K0199, 80NAAC21K0014, NNX17AG69G, 80NSSC22K0170, 80NSSC22K0016, and NSF grant AGS-2120511. YZ is supported by NASA grants 80NSSC20K0354, 80NSSC21K1673, and NNX15AB83G. The National Center for Atmospheric Research is sponsored by the National Science Foundation.

References

Anderson, P. C. (2004). Subauroral electric fields and magnetospheric convection during the April, 2002 geomagnetic storms. *Geophysical Research Letters*, *31*, L11801. https://doi.org/10.1029/2004GL019588

Anderson, P. C., Hanson, W. B., Heelis, R. A., Craven, J. D., Baker, D. N., & Frank, L. A. (1993). A proposed production model of rapid subauroral ion drifts and their relationship to substorm evolution. *Journal of Geophysical Research*, *98*(A4), 6069–6078. https://doi.org/10.1029/92ja01975

Brace, L. H., Chappell, C. R., Chandler, M. O., Comfort, R. H., Horwitz, J. L., & Hoegy, W. R. (1988). *F* region electron temperature signatures of the plasmapause based on Dynamics Explorer 1 and 2 measurements. *Journal of Geophysical Research*, *93*(A3), 1896–1908. https://doi.org/10.1029/JA093iA03p01896

Brace, L. H., Maier, E. J., Hoffman, J. H., Whitteker, J., & Shepherd, G. G. (1974). Deformation of the night side plasmasphere and ionosphere during the August 1972 geomagnetic storm. *Journal of Geophysical Research*, *79*(34), 5211–5218. https://doi.org/10.1029/JA079i034p05211

Cornwall, J. M., Coroniti, F. V., & Thorne, R. M. (1971). Unified theory of SAR arc formation at the plasmapause. *Journal of Geophysical Research*, *76*(19), 4428–4445. https://doi.org/10.1029/JA076i019p04428

Evans, J. V. (1965). Cause of the midlatitude winter night increase in f_0F_2. *Journal of Geophysical Research*, *70*(17), 4331–4345. https://doi.org/10.1029/JZ070i017p04331

Fejer, B. G., Jensen, J. W., & Su, S.-Y. (2008). Quiet time equatorial F region vertical plasma drift model derived from ROCSAT-1 observations. *Journal of Geophysical Research*, *113*, A05304. https://doi.org/10.1029/2007JA012801

Foster, J. C. (1993). Storm time plasma transport at middle and high latitudes. *Journal of Geophysical Research*, *98*(A2), 1675–1689. https://doi.org/10.1029/92JA02032

Foster, J. C., & Burke, W. J. (2002). SAPS: A new characterization for sub-auroral electric fields. *Eos Transactions American Geophysical Union*, *83*, 393–394. https://doi.org/10.1029/2002eo000289

Foster, J. C., & Vo, H. B. (2002). Average characteristics and activity dependence of the subauroral polarization stream. *Journal of Geophysical Research*, *107*(A12), SIA16-1–SIA16-10. https://doi.org/10.1029/2002JA009409

Gussenhoven, M. S., Hardy, D. A., & Heinemann, N. (1983). Systematics of the equatorward diffuse auroral boundary. *Journal of Geophysical Research*, *88*(A7), 5692–5708. https://doi.org/10.1029/JA088iA07p05692

Hardy, D. A., Gussenhoven, M. S., & Holeman, E. (1985). A statistical model of auroral electron precipitation. *Journal of Geophysical Research*, *90*(A5), 4229–4248. https://doi.org/10.1029/JA090iA05p04229

Horvath, I., & Lovell, B. C. (2021). Investigating the coupled magnetosphere-ionosphere-thermosphere (M-I-T) system's responses to the 20 November 2003 Superstorm. *Journal of Geophysical Research: Space Physics*, *126*, e2021JA029215. https://doi.org/10.1029/2021JA029215

Huang, C.-S. (2020). Westward plasma drifts in the nighttime equatorial ionosphere during severe magnetic storms: A new type of penetration electric fields caused by subauroral polarization stream. *Journal of Geophysical Research: Space Physics*, *125*, e2020JA028300. https://doi.org/10.1029/2020JA028300

Huang, C.-S., Zhang, Y., Wang, W., Lin, D., & Wu, Q. (2021). Low-latitude zonal ion drifts and their relationship with subauroral polarization streams and auroral return flows during intense magnetic storms. *Journal of Geophysical Research: Space Physics*, *126*, e2021JA030001. https://doi.org/10.1029/2021JA030001

Immel, T. J., Sagawa, E., England, S. L., Henderson, S. B., Hagan, M. E., Mende, S. B., et al. (2006). Control of equatorial ionospheric morphology by atmospheric tides. *Geophysical Research Letters*, *33*, L15108. https://doi.org/10.1029/2006GL026161

Jordanova, V. K., Farrugia, C. J., Thorne, R. M., Khazanov, G. V., Reeves, G. D., & Thomsen, M. F. (2001). Modeling ring current proton precipitation by electromagnetic ion cyclotron waves during the May 14–16, 1997, storm. *Journal of Geophysical Research*, *106*(A1), 7–22. https://doi.org/10.1029/2000JA002008

Kozyra, J. U., Brace, L. H., Cravens, T. E., & Nagy, A. F. (1986). A statistical study of the subauroral electron temperature enhancement using Dynamics Explorer 2 Langmuir probe observations. *Journal of Geophysical Research*, *91*(A10), 11270–11280. https://doi.org/10.1029/JA091iA10p11270

Kozyra, J. U., Shelley, E. G., Comfort, R. H., Brace, L. H., Cravens, T. E., & Nagy, A. F. (1987). The role of ring current O^+ in the formation of stable auroral red arcs. *Journal of Geophysical Research*, *92*(A7), 7487–7502. https://doi.org/10.1029/JA092iA07p07487

Lee, I. T., Wang, W., Liu, J. Y., Chen, C. Y., & Lin, C. H. (2011). The ionospheric midlatitude trough observed by FORMOSAT-3/COSMIC during solar minimum. *Journal of Geophysical Research*, *116*, A06311. https://doi.org/10.1029/2010JA015544

Mallis, M., & Essex, E. A. (1993). Diurnal and seasonal variability of the southern-hemisphere main ionospheric trough from differential-phase measurements. *Journal of Atmospheric and Terrestrial Physics*, *55*, 1021–1037. https://doi.org/10.1016/0021-9169(93)90095-g

Mishin, E. V., & Burke, W. J. (2005). Stormtime coupling of the ring current, plasmasphere, and topside ionosphere: Electromagnetic and plasma disturbances. *Journal of Geophysical Research*, *110*(A7), A07209. https://doi.org/10.1029/2005JA011021

Moffett, R. J., & Quegan, S. (1983). The mid-latitude trough in the electron concentration of the ionospheric F-layer: A review of observations and modelling. *Journal of Atmospheric and Terrestrial Physics*, *45*, 315–343. https://doi.org/10.1016/s0021-9169(83)80038-5

Nagata, K., Kohno, T., Murakami, H., Nakamoto, A., Hasebe, N., Kikuchi, J., & Doke, T. (1988). Electron (0.19-3.2 MeV) and proton (0.58-35 MeV) precipitations observed by OHZORA satellite at low latitude zones $L = 1.6$-1.8. *Planetary and Space Science*, *36*(6), 591–606. https://doi.org/10.1016/0032-0633(88)90028-1

Newell, P. T., Sotirelis, T., Liou, K., Meng, C.-I., & Rich, F. J. (2007). A nearly universal solar wind-magnetosphere coupling function inferred from 10 magnetospheric state variables. *Journal of Geophysical Research*, *112*, A01206. https://doi.org/10.1029/2006JA012015

Oyama, K.-I., Balan, N., Watanabe, S., Takahashi, T., Isoda, F., Bailey, G. J., & Oya, H. (1996). Morning overshoot of Te enhanced by downward plasma drift in the equatorial topside ionosphere. *Journal of Geomagnetism and Geoelectricity*, *48*, 959–966. https://doi.org/10.5636/jgg.48.959

Prölss, G. W. (2006). Subauroral electron temperature enhancement in the nighttime ionosphere. *Annals of Geophysics*, *24*, 1871–1885. https://doi.org/10.5194/angeo-24-1871-2006

Prölss, G. W. (2007). The equatorward wall of the subauroral trough in the afternoon/evening sector. *Annals of Geophysics*, *25*, 645–659. Retrieved from www.ann-geophys.net/25/645/2007/

Rich, F. J. (1994). *Users Guide for Topside Ionospheric Plasma Monitor (SSIES, SSIES-2, and SSIES-3) on Spacecraft of the Defense Meteorological Satellite Program (DMSP)* (Vol. *I*), Technical description, PL-TR-94-2187, Environmental Research Papers, No. 1151. Retrieved from http://cedar.openmadrigal.org/static/siteSpecific/users_guide_dmsp_rich.pdf

Schunk, R. W., & Nagy, A. F. (1978). Electron temperatures in the F region of the ionosphere: Theory and observations. *Reviews of Geophysics*, *16*(3), 355–399. https://doi.org/10.1029/RG016i003p00355

Schunk, R. W., & Nagy, A. F. (1980). Ionospheres of the terrestrial planets. *Reviews of Geophysics*, *18*(4), 813–852. https://doi.org/10.1029/RG018i004p00813

Stolle, C., Liu, H., Truhlík, V., Lühr, H., & Richards, P. G. (2011). Solar flux variation of the electron temperature morning overshoot in the equatorial F region. *Journal of Geophysical Research*, *116*, A04308. https://doi.org/10.1029/2010JA016235

Sultan, P. J., & Rich, F. J. (2001). Validation of in Situ ionospheric density measurements with Ground-based radar. *Journal of Spacecraft and Rockets*, *38*(4), 590–593. https://doi.org/10.2514/2.3721

Thorne, R. M., & Horne, R. B. (1992). The contribution of ion-cyclotron waves to electron heating and SAR-arc excitation near the storm-time plasmapause. *Geophysical Research Letters*, *19*(4), 417–420. https://doi.org/10.1029/92GL00089

Zhang, S.-R., Holt, J. M., Zalucha, A. M., & Amory-Mazaudier, C. (2004). Midlatitude ionospheric plasma temperature climatology and empirical model based on Saint Santin incoherent scatter radar data from 1966 to 1987. *Journal of Geophysical Research*, *109*, A11311. https://doi.org/10.1029/2004JA010709

Zhang, S.-R., Zhang, Y., Wang, W., & Verkhoglyadova, O. P. (2017). Geospace system responses to the St. Patrick's Day storms in 2013 and 2015. *Journal of Geophysical Research: Space Physics*, *122*, 6901–6906. https://doi.org/10.1002/2017JA024232

Zhang, Y., Paxton, L. J., Morrison, D., Wolven, B., Kil, H., Meng, C.-I., et al. (2004). O/N2 changes during 1–4 October 2002 storms: IMAGE SI-13 and TIMED/GUVI observations. *Journal of Geophysical Research*, *109*, A10308. https://doi.org/10.1029/2004JA010441

Zhong, J., Lei, J., Yue, X., Luan, X., & Dou, X. (2019). Middle-latitudinal band structure observed in the nighttime ionosphere. *Journal of Geophysical Research: Space Physics*, *124*, 5857–5873. https://doi.org/10.1029/2018JA026059